Biogeosciences Discuss., https://doi.org/10.5194/bg-2018-118
Manuscript under review for journal Biogeosciences
Discussion started: 9 April 2018

Biogeosciences Discussions Open Access EGU

Latitudinal variations of $\delta^{30}Si$ and $\delta^{15}N$ signatures along the Peruvian shelf: quantifying the effects of nutrient utilization versus denitrification over the past 600 years

Kristin Doering[1], Claudia Ehlert[2], Philippe Martinez[3], Martin Frank[1], Ralph Schneider[4]

[1]GEOMAR Helmholtz Centre for Ocean Research Kiel, Kiel, 24148, Germany
[2]Max Planck Research Group - Marine Isotope Geochemistry, Carl von Ossietzky University, 26129 Oldenburg, Germany
[3]EPOC, UMR CNRS 5805, Université de Bordeaux 1, 33615 Pessac Cedex, France
[4]Institute of Geosciences, University of Kiel, Kiel, 24118, Germany

Correspondence to: Kristin Doering (kdoering@geomar.de)

Abstract

The sedimentary stable nitrogen isotope compositions of bulk organic matter ($\delta^{15}N_{bulk}$) and silicon isotope composition of diatoms ($\delta^{30}Si_{BSi}$) both mainly reflect the degree of past nutrient utilization by primary producers. However, in ocean areas where anoxic and suboxic conditions prevail, the $\delta^{15}N_{bulk}$ signal ultimately recorded within the sediments is also influenced by water column denitrification causing an increase in the subsurface $\delta^{15}N$ signature of dissolved nitrate ($\delta^{15}NO_3^-$) upwelled to the surface. Such conditions are found in the oxygen minimum zone off Peru, where at present an increase in subsurface $\delta^{15}NO_3^-$ from North to South along the shelf is observed due to ongoing denitrification within the pole-ward flowing subsurface waters, while the $\delta^{30}Si$ signature of silicic acid ($\delta^{30}Si(OH)_4$) at the same time remains unchanged.

Here, we present three new $\delta^{30}Si_{BSi}$ records between 11°S and 15°S and compare these to previously published $\delta^{30}Si_{BSi}$ and $\delta^{15}N_{bulk}$ records from Peru covering the past 600 years. We present a new approach to calculate past subsurface $\delta^{15}NO_3^-$ signatures based on the correlation of $\delta^{30}Si_{BSi}$ and $\delta^{15}N_{bulk}$ signatures at a latitudinal resolution for different time periods. Our results show source water $\delta^{15}NO_3^-$ compositions during the last 200 years, the Current Warm Period (CWP) and during short-term arid events prior to that, which are close to modern values increasing southward from 7 to 10‰ (between 11°S and 15°S). In contrast, humid conditions during the Little Ice Age (LIA) reflect consistently low $\delta^{15}NO_3^-$ values between 6 and 7.5‰. Furthermore, we are able to relate the short-term variability in both isotope compositions to changes in the ratio of nutrients (NO_3^-: $Si(OH)_4$) taken up by different dominating phytoplankton groups (diatoms and non-siliceous phytoplankton) under the variable climatic conditions of the past 600 years.

1. Introduction

Investigations of the isotopic compositions of the macro-nutrients, such as $Si(OH)_4$ and NO_3^-, have been used to infer changes of biogeochemical cycles in the past (Brunelle et al., 2007; Horn et al.,

2011; Robinson et al., 2014). The preferential incorporation of the lighter isotopes ^{14}N and ^{28}Si into organic matter (OM) and biogenic opal (BSi), respectively, during primary production in surface waters leads to an increase in the $\delta^{15}N$ and $\delta^{30}Si$ in the remaining dissolved nutrients (i.e. $\delta^{15}NO_3^-$ and $\delta^{30}Si(OH)_4$) as a results of progressive consumption of the nutrient pools (Altabet et al., 1991; De La Rocha et al., 1997; Wada and Hattori, 1978). This preferential incorporation is associated with an approximate enrichment factor of -5‰ for NO_3^- (Waser et al., 1998) and -1.1‰ for $Si(OH)_4$ (De La Rocha et al., 1997). Accordingly, the degree of utilization of NO_3^- and $Si(OH)_4$ is recorded in the $\delta^{15}N_{bulk}$ and $\delta^{30}Si_{BSi}$ of the OM and BSi produced. In combination with parameters such as organic carbon, BSi or barium accumulation rates, both $\delta^{15}N_{bulk}$ and $\delta^{30}Si_{BSi}$ have been employed as proxies for the evaluation of past productivity and corresponding nutrient utilization (De La Rocha et al., 1998; François et al., 1992; Horn et al., 2011; Pichevin et al., 2005).

However, in coastal upwelling areas, where upwelling of nutrient-rich subsurface waters causes high surface productivity, subsequent degradation of the high amounts of OM leads to extensive oxygen consumption in the water column (Pennington et al., 2006; Zuta and Guillén, 1970). As a result of the low oxygen concentrations, NO_3^- is used as an oxidant during OM degradation and is transferred to N_2 leading to a net loss of bio-available nitrogen (e.g., denitrification and anaerobe ammonium-oxidation; Codispoti, 2006; Lam et al., 2009). Due to the high isotope fractionation factor (~20‰) associated with denitrification, the $\delta^{15}NO_3^-$ signatures of subsurface waters strongly increase and consequently supply a heavy $\delta^{15}NO_3^-$ signal to surface waters during upwelling (Cline and Kaplan, 1975). This ^{15}N-enriched NO_3^- is incorporated by phytoplankton and ultimately deposited and buried in marine sediments. Accordingly, although $\delta^{15}N_{bulk}$ also varied in phase with productivity proxies, elevated $\delta^{15}N_{bulk}$ values in highly productive and poorly ventilated regions including most of the coastal upwelling areas, have been generally interpreted as the consequence of stronger denitrification associated with intense oxygen depletion (Agnihotri et al., 2006; 2008; De Pol-Holz et al., 2007; Fleury et al., 2015; Gutiérrez et al., 2009; Mollier-Vogel et al., 2012; Salvatteci et al., 2014b). However, given that dissolved $\delta^{15}NO_3^-$ is influenced by both nutrient utilization and denitrification – associated with water column de-oxygenation - both processes should also influence the $\delta^{15}N_{bulk}$ signatures recorded by the sedimentary OM.

In contrast, $\delta^{30}Si_{BSi}$ signatures are primarily controlled by surface water diatom productivity and $Si(OH)_4$ utilization (Brzezinski, 2002; De La Rocha et al., 1998) closely coupled to the amount of upwelling strength in the study area (Doering et al., 2016; Ehlert et al., 2012; 2013; 2015; Grasse et al., 2013). Thus, the combination of both $\delta^{30}Si_{BSi}$ and $\delta^{15}N_{bulk}$ compositions in the water column and late Quaternary sediments off Peru has been applied as a measure to disentangle modern and past nutrient utilization and denitrification processes (Ehlert et al., 2015; Grasse et al., 2016). Comparison of modern dissolved $Si(OH)_4$ and NO_3^- distributions and their corresponding isotopic ratios has shown that $Si(OH)_4$ and NO_3^- concentrations and the stable isotopic signatures are strongly correlated within the surface mixed layer at near-shore and offshore areas, indicating that the signal preserved in the sediments mainly depends on the degree of utilization of both nutrients (Grasse et al., 2016). Similarly, an initial comparison for the past 600 years based on one sediment core indicated that both isotope compositions were mainly influenced by nutrient utilization suggesting that denitrification was not the

main control on past isotopic variations (Ehlert et al., 2015) thus partly contradicting previous interpretations of N-loss having been the main driver of changes in past $\delta^{15}N_{bulk}$ records.

Today, the dissolved $\delta^{15}NO_3^-$ signatures increase southward along the Peruvian margin due to the continuous enrichment in ^{15}N by denitrification in pole-ward flowing subsurface waters (Mollier-Vogel et al., 2012), while $\delta^{30}Si(OH)_4$ values remain stable. Here, our goal is to verify whether this southward increase of $\delta^{15}NO_3^-$ due to denitrification has been persisted during the marked changes in upwelling intensity of the past ~600 years based on correlation of $\delta^{30}Si_{BSi}$ and $\delta^{15}N_{bulk}$ signatures of four different sediment cores retrieved along the entire gradient of upwelling strength of the southern Peruvian shelf. More specifically, we aim to detect the extent of variability in $\delta^{15}N_{bulk}$ caused as a function of denitrification and nutrient utilization during specific time periods (i.e. Current Warm Period (CWP) and Little Ice Age (LIA)). Therefore, we present three new records for $\delta^{30}Si_{BSi}$ and BSi concentrations from the Peruvian shelf between 11°S and 15°S covering the last 600 to 1000 years BP. These are compared to previously published $\delta^{15}N_{bulk}$ data obtained from the same cores (Fleury et al., 2015) and to$\delta^{30}Si_{BSi}$ and $\delta^{15}N_{bulk}$ records from a fourth core from 14°S (Ehlert et al., 2015)(Fig.1).

Regional Setting

Along the Peruvian margin the main source for the high amounts of upwelled nutrients is the subsurface Peru-Chile Undercurrent (PCUC), which flows southward along the continental slope and outer shelf between 4°S and 14°S at a depth between 50 and 150 m, before it detaches from the shelf south of 15°S (Brink et al., 1983; Chaigneau et al., 2013; Toggweiler et al., 1991). Eastward flowing subsurface waters of the Equatorial Undercurrent (EUC) and the Southern Subsurface Counter Current (SSCC) (see Fig. 1a) feed the PCUC. These subsurface currents deliver $Si(OH)_4$ and NO_3^- with mean preformed source signatures for $\delta^{30}Si(OH)_4$ of 1.5 ± 0.2‰ (Beucher et al., 2011; Ehlert et al., 2012; Grasse et al., 2013) and for $\delta^{15}NO_3^-$ of 7.1 ± 0.3‰ for the EUC. Within the SSCC preformed $\delta^{15}NO_3^-$ values of 5.5 ± 0.3‰ for (Rafter et al., 2012) are slightly lower, resulting in an approximate average PCUC value of ~6‰ (Fig. 2a; Mollier-Vogel et al., 2012).

The modern surface sediment $\delta^{15}N_{bulk}$ and $\delta^{30}Si_{BSi}$ compositions both reflect an increase from North to South (Fig. 2a). However, only the dissolved $\delta^{15}NO_3^-$ of subsurface waters (50-150 m water depth) increases southward from 6‰ to 15.5‰ (EQ to 17°S; Mollier-Vogel et al., 2012) as a consequence of water column denitrification, while the dissolved $\delta^{30}Si(OH)_4$ signature remains close to the source value of 1.5‰ for the PCUC (50-150 m water depth; Fig. 2a; Ehlert et al., 2012). This difference in the evolution of the isotopic signature from North to South is caused by the anoxic conditions off Peru only increasing the $\delta^{15}NO_3^-$ signatures via denitrification in the subsurface, but not the $\delta^{30}Si(OH)_4$ signatures. Accordingly, at the northern shelf between 1°N and 10°S, where subsurface O_2 concentrations [O_2] are >20 µmol L^{-1}, N-loss is not observed and the $\delta^{15}N_{bulk}$ values in the sediments range between 4 and 5‰ close to the source value of 6‰ of $\delta^{15}NO_3^-$, thus indicating a high degree of NO_3^- utilization (70-80%; Fig. 2b; Mollier-Vogel et al., 2012). In contrast, the $\delta^{30}Si_{BSi}$ signatures north of 10°S are highly variable (0.3-0.9‰) reflecting an overall lower degree of utilization (20-40%; Doering et al., 2016; Ehlert et al., 2012) (Please note that all Si and N utilization calculations

are based on an open steady-state system). At the central Peruvian shelf (10-12°S), where subsurface [O_2] is <20 µmol L^{-1} (Fig. 2a), the subsurface source value of $\delta^{15}NO_3^-$ increases to 8.6‰ due to denitrification (Mollier-Vogel et al., 2012). The $\delta^{30}Si_{BSi}$ and $\delta^{15}N_{bulk}$ values both increase to 0.9 ± 0.1‰ and 6.1 ± 0.8‰, respectively, reflecting higher $Si(OH)_4$ utilization (20-60%) but lower NO_3^- utilization (15-65%, Fig. 2b) associated with increased upwelling intensity, high nutrient re-supply and higher consumption via diatom productivity. In the southernmost part of the shelf (13-16°S) highest productivity and upwelling intensity prevail, leading to a further increase in the subsurface $\delta^{15}NO_3^-$ signature of up to 12.5‰ at 15°S (southernmost surface sediment station of the study area), whereas surface sediment mean $\delta^{30}Si_{BSi}$ and $\delta^{15}N_{bulk}$ values further increase to 1.1 ± 0.1‰ and 8.9 ± 1.4‰ reflecting moderate $Si(OH)_4$ utilization of 50-70% ($\delta^{30}Si_{BSi}$) and NO_3^- utilization of 20-70% ($\delta^{15}N_{bulk}$). The supply for dissolved $Si(OH)_4$ strongly increases from the northern shelf to the southern shelf area (Fig. 2c), reflecting the strongest upwelling conditions. This increase in upwelling and productivity between 10-15°S is reflected by the high sedimentary concentrations of BSi (10-17%; Ehlert et al., 2012) and total nitrogen (TN, 0.8-1.2%; Mollier-Vogel et al., 2012). However, the NO_3^- supply, as indicated by subsurface (50-150 m) NO_3^- concentrations, slightly decreases from North to South, reflecting the loss of NO_3^- via denitrification and anammox.

2. Material and Methods

2.1 Core locations and age models

The new data in this study were obtained from three short, fine-laminated trigger cores retrieved from the main upwelling region off the Peruvian margin during the German R/V Meteor cruise M77/2 in 2008 as part of the Collaborative Research Center (SFB) 754. New records of $\delta^{30}Si_{BSi}$ and BSi concentrations were generated for cores M77/2-024-5TC (024-5TC; 11°05'S, 78°00'W, 210 m water depth), M77/2-005-3TC (005-3TC; 12°05'S, 77°40'W, 214 m water depth) and core M77/2-003-2TC (003-2TC; 15°06'S, 75°41'W, 271 m water depth). Core locations are shown in Fig. 1b. The age models were published before in study of Fleury et al. (2015). The age models for all cores are given years BP, with BP relating to 2008.

2.2 Biogenic opal and silicon isotope analyses

The amount of BSi in the sediments was measured following an automated leaching method using sodium hydroxide (DeMaster, 1981; Müller and Schneider, 1993) with a precision of 1-2% (1 SD).

For the silicon isotope measurements diatoms were extracted from the sediment by chemical and physical cleaning (11 and 32 µm sieve; heavy liquid separation with a sodium polytungstate solution set at 2.15 g mL^{-1}) as described in detail in Ehlert et al. (2012; 2013) and Doering et al. (2016). For all samples the purity of the small diatom fraction (11-32 µm) was evaluated via light microscopy prior to dissolution and only pure (>95%) diatom samples were treated further. All samples were dissolved in 1 mL 0.1 M NaOH and treated with 200 µL concentrated H_2O_2 (Suprapur). Sample solutions were diluted with 4 mL MQ water and neutralized with 0.1 mL 1 M HCl (Reynolds et al., 2008), followed by a chromatographic purification using 1 mL pre-cleaned AG50W-X8 cation

exchange resin (BioRad, mesh 200-400) (de Souza et al., 2012). The Si isotopic compositions were determined in 0.6 ppm sample solutions on a *NuPlasma HR* MC-ICPMS at GEOMAR applying a standard-sample bracketing method (Albarède et al., 2004). Silicon isotopic compositions are reported in the δ-notation relative to the reference standard NBS28 in parts per thousand: $\delta^{30}Si = ((R_{sample}/R_{standard})-1)*1000$, where R_{sample} is the $^{30}Si/^{28}Si$ ratio of the sample and $R_{standard}$ is the $^{30}Si/^{28}Si$ ratio of the NBS28. All $\delta^{30}Si$ measurements were run at least in triplicates, with uncertainties ranging between 0.05‰ and 0.27‰ (2 SD). Repeated measurements of an in-house matrix standard gave average $\delta^{30}Si$ values of 1.03 ± 0.21‰ (2 SD, n=15). Long-term repeated measurements of the reference materials NBS28, IRMM018, and Big Batch gave average $\delta^{30}Si$ values of 0.00 ± 0.24‰ (2 SD, n=15), -1.40 ± 0.21‰ (2 SD, n=15) and -10.60 ± 0.24‰ (2 SD, n=15), respectively, in good agreement with literature values (Reynolds et al., 2007).

3. Results and discussion

The climate of the last 600 years is divided into two climatic phases consisting of the CWP (200 years BP to present) and the LIA (600-200 years BP). Off Peru, the CWP has been characterized by dry (arid) conditions, high upwelling intensity, as well as high productivity and strong N-loss processes, reflecting overall dominant La-Niña conditions (Fleury et al., 2015; Salvatteci et al., 2014b; Sifeddine et al., 2008). In contrast, the LIA has been shown to be characterized by lower productivity and low denitrification intensity for the present day main upwelling area between 10°S and 15°S (Díaz-Ochoa et al., 2009; Salvatteci et al., 2014b; Sifeddine et al., 2008). Such conditions are more similar to modern El-Niño events in the area and thus generally referred to as El-Niño-like conditions (Clement et al., 2000). Previous paleo-reconstructions agreed that the latter conditions were a consequence of larger scale climatic changes induced by weakening of the Walker circulation and reduction of the South Pacific subtropical High (SPSH), as well as by a southward shift of the mean position of the Intertropical Convergence Zone (ITCZ) and the associated precipitation belt (Fleury et al., 2015; Sachs et al., 2009; Salvatteci et al., 2014b; Sifeddine et al., 2008). This was inferred to result in a deepening of the nutricline and reduced surface productivity and more oxygenated subsurface waters, as indicated by lower BSi and TOC concentrations (*this study*; Ehlert et al., 2015; Gutiérrez et al., 2009; Salvatteci et al., 2014a) and Si/Fe ratios (Fleury et al., 2015). Conditions which are supported by a marked reduction in the concentrations of sedimentary redox sensitive trace metals such as molybdenum and rhenium (Salvatteci et al., 2014b; Sifeddine et al., 2008). However, these conditions were not constant at all. Short-term variations during both periods are reflected for example by changes in diatom abundances, productivity sensitive elements (Br/Fe) and $\delta^{15}N_{bulk}$ values (Fleury et al., 2015). These proxy records probably indicate multidecadal shifts between arid/humid conditions during the CWP and particularly the LIA during which marked short-term periods of arid conditions occurred (Fleury et al., 2015) (Fig. 3).

The well-studied biogeochemical evolution of the Peruvian shelf over the last 600 years and the significant differences in productivity and subsurface oxygenation between the CWP and the LIA

Biogeosciences Discuss., https://doi.org/10.5194/bg-2018-118
Manuscript under review for journal Biogeosciences
Discussion started: 9 April 2018

are the basis for our study to gain new insights into the relationship between nutrient utilization and denitrification via $\delta^{30}Si_{BSi}$ and $\delta^{15}N_{bulk}$ records.

3.1 Changes in BSi production and $\delta^{30}Si_{BSi}$ during the last 600 years

The data of the sediment cores from the shelf area between 12°S and 15°S presented here show an increase in BSi content from mean values of 13-23% during the LIA to values of 21-29% during the CWP. The $\delta^{30}Si$ records follow a similar trend of lower mean $\delta^{30}Si_{BSi}$ values of around 0.8 to 1‰ during the LIA to higher mean values of 1 to 1.5‰ during the CWP. This indicates that diatom productivity and $Si(OH)_4$ utilization, reconstructed via BSi concentrations and $\delta^{30}Si_{BSi}$ values, most of the time were lower during the LIA than during the CWP (Fig. 3; Table 1).

Overall the BSi concentrations and $\delta^{30}Si_{BSi}$ signatures at 12°S (005-3TC) and 15°S (003-2TC) are lowest during the LIA (Fig. 3c,e), in agreement with previously published records from 11°S (M77/1-470) and 14°S (B0405-6; Ehlert et al., 2015). An exception is core 024-5TC from 11°S, where $\delta^{30}Si$ mean values of the LIA (1.3 ± 0.4‰) are similar to CWP mean values (1.4 ± 0.1‰). Furthermore, both the BSi concentrations and $\delta^{30}Si_{BSi}$ of core 024-5TC are significantly higher during the LIA than at nearby core M77/1-470 (Fig. 2a; Ehlert et al. 2015). Such consistently high BSi and $\delta^{30}Si$ values may be explained by limited $Si(OH)_4$ supply at site 024-5TC during the LIA resulting in a higher degree of $Si(OH)_4$ utilization. This is, however, not supported by other productivity proxies such as the Si/Fe ratio and the total diatom abundance for core 024-5TC, which do not indicate similarly high BSi production during the LIA and the CWP (Fleury et al., 2015). The finely laminated sediments do indicate short periods of higher productivity during the LIA in phase with more arid conditions (Fig. 3, grey shadings; for details see (Fleury et al., 2015). Accordingly, the high mean BSi and $\delta^{30}Si_{BSi}$ values obtained from core 024-5TC may be an artifact of the low sampling resolution with only two $\delta^{30}Si_{BSi}$ samples between 200 and 350 years BP. Alternatively, the increase in $Si(OH)_4$ utilization decoupled from an increase in diatom abundance (data by Fleury et al. (2015) not shown here) may indicate stronger silicification of the diatom frustules, as often observed under iron (Fe)-deficient conditions further associated with an increase in the $Si(OH)_4$:NO_3^- incorporated by the diatoms (De La Rocha et al., 2000; Takeda, 1998; Wilken et al., 2011).

As previously shown the $\delta^{15}N_{bulk}$ values of the three cores (M77/2-024-5TC, 005-3TC and 003-2TC) presented in this study were on average lower during the LIA than during the CWP (Fleury et al., 2015). The $\delta^{15}N_{bulk}$ values reported for core 005-3TC (12°S) are close to values of nearby core B0406-13 (Gutiérrez et al., 2009). Similarly, the $\delta^{15}N_{bulk}$ values of core 003-2TC (15°S) agree well with previously published $\delta^{15}N_{bulk}$ record of core B0405-6 (14°S, Fig. 3 c, d; Gutiérrez et al., 2009); Overall, productivity and nutrient utilization proxies (BSi and $\delta^{30}Si_{BSi}$) varied in phase with $\delta^{15}N_{bulk}$ signatures at all core locations (Fig. 3).

3.2 Impact of denitrification versus nutrient utilization on the records

Given the significant changes in upwelling intensity, productivity and subsurface oxygenation (and thus N-loss) between the LIA and CWP (Fig. 3), we first investigate if and how the preformed $\delta^{15}NO_3^-$

Biogeosciences Discuss., https://doi.org/10.5194/bg-2018-118
Manuscript under review for journal Biogeosciences
Discussion started: 9 April 2018

225 signal changed with latitude (between 11°S and 15°S), and then uses this information to reconstruct
226 how nutrient supply and utilization changed during these time periods.

227 To disentangle denitrification and relative nutrient utilization we apply a correlation of $\delta^{30}Si_{BSi}$
228 and $\delta^{15}N_{bulk}$ values based on observations from today's surface sediments (Fig. 4a). Despite that
229 denitrification strongly increases the $\delta^{15}NO_3^-$ values in subsurface waters ultimately upwelled to the
230 surface and incorporated into phytoplankton, modern sediment values of $\delta^{15}N_{bulk}$ are mainly controlled
231 by the degree of surface water NO_3^- utilization (Ehlert et al., 2015; Mollier-Vogel et al., 2012).
232 Particularly between 10°S and 17°S, where the subsurface $\delta^{15}NO_3^-$ source value increases southward
233 due to increasing O_2 deficit and increasing denitrification, the $\delta^{30}Si_{BSi}$ and $\delta^{15}N_{bulk}$ values are generally
234 close to the 1:1 utilization line indicating a similar uptake efficiency of both NO_3^- and $Si(OH)_4$,
235 respectively (Fig. 4a). This is in agreement with observations from modern water samples, for which
236 nutrient ratios (NO_3^-:$Si(OH)_4$) near the shelf were found to be close to 1:1 (varying between 1:2 and
237 2:1) (Grasse et al., 2016). Accordingly, the surface sediment $\delta^{30}Si_{BSi}$ versus $\delta^{15}N_{bulk}$ signatures illustrate
238 the southward increase in source $\delta^{15}NO_3^-$ signatures (Fig. 4a; stars), but remain close to the respective
239 1:1 utilization line for NO_3^-:$Si(OH)_4$.

240 The linear relationship between $\delta^{30}Si_{BSi}$ and $\delta^{15}N_{bulk}$ should thus also be a direct indicator of
241 the $\delta^{15}NO_3^-$ source signatures in the past during the CWP and the LIA. In order to estimate past
242 changes in the $\delta^{15}NO_3^-$ source values the $\delta^{30}Si_{BSi}$ and $\delta^{15}N_{bulk}$ values for both time periods were
243 separately plotted against each other (Fig. 4c-e) and $\delta^{15}NO_3^-$ was calculated based on the linear
244 function assuming that the source $\delta^{30}Si(OH)_4$ signature always remained stable at 1.5‰ over time:

245 (1) $\delta^{30}Si(OH)_4 = a * \delta^{15}NO_3^- + b$, or

246 (2) $\delta^{15}NO_3^- = \left(\delta^{30}Si(OH)_4 - b\right)/a$

247 with *a* indicating the slope of the line and b the intercept. Accordingly, we calculated the linear
248 regression based on all samples of the different cores from the different latitudes (11°S, 12° S, 14°S
249 and 15°S) during the CWP and LIA. We also further differentiated between short-term productive
250 phases (arid phases) and the generally prevailing humid El-Niño like conditions during the LIA (grey
251 shadings in Fig. 3), and resolved the resulting equation based on eq. (2) to estimate $\delta^{15}NO_3^-$.

252 The degree of nutrient utilization can be described assuming either Rayleigh-type (single input
253 followed by no additional nutrients newly supplied to a particular parcel of water followed by
254 fractional loss as a function of production and export) or steady-state (continuous supply and partial
255 consumption of nutrients causing a dynamic equilibrium of the dissolved nutrient concentration and the
256 product) fractionation behavior (Mariotti et al., 1981). For means of simplification we will only provide
257 the values derived from steady state fractionation, which was shown to better reflect upwelling
258 conditions off Peru (Ehlert et al., 2012).

259 (3) $\%Si(OH)_{4\,consumed} = 1 - \left(\left(\delta^{30}Si - \delta^{30}Si(OH)_{4\,source}\right)/^{30}\varepsilon\right) * 100$ or

$\%NO_3^-{}_{consumed} = [1 - \left(\delta^{15}N - \delta^{15}NO_3^-\right)/^{15}\varepsilon] * 100$

260 with $\%Si(OH)_{4\,consumed}$ or $\%NO_3^-{}_{consumed}$ being the percentages of the supplied $Si(OH)_4$ and NO_3^- that
261 have been utilized. For this calculation we apply enrichment factors of −1.1‰ $^{30}\varepsilon$ ($\delta^{30}Si$, De La Rocha
262 et al., 1997) and −5‰ $^{15}\varepsilon$ ($\delta^{15}N$) and assume a constant source water signature of 1.5‰ for $\delta^{30}Si(OH)_4$

$_{source}$ (i.e. the mean $\delta^{30}Si(OH)_4$ of the PCUC). The impact of denitrification on the $\delta^{15}NO_3^-$ signatures of the past is assessed in the following section before calculating past NO_3^- utilization for the respective latitudes.

3.2.1 Disentangling nutrient utilization and N-loss processes: Changes in the source water nitrate isotopic composition

To study the importance of utilization and denitrification during the CWP and LIA we reconstructed nutrient utilization at the different core sites by assessing the deviation from 1:1 (NO_3^-:$Si(OH)_4$) utilization over time based on the direct comparison of $\delta^{30}Si_{BSi}$ and $\delta^{15}N_{bulk}$ values. Under the influence of denitrification (N-loss) the isotopic value of NO_3^- in the source waters will be shifted to higher values.

Our results show that the correlation of $\delta^{30}Si_{BSi}$ to $\delta^{15}N_{bulk}$ during the CWP is comparable to modern values between 10°S and 15°S (Figs. 4a,b). The isotopic compositions of samples from all cores generally plot close to the 1:1 utilization lines indicating a $\delta^{15}NO_3^-$ source value of 8 to 9‰, similar to present day subsurface waters between 10°S and 15°S (Fig. 4a,b). Furthermore, the $\delta^{15}N_{bulk}$ values and calculated subsurface $\delta^{15}NO_3^-$ source values indicate a similar southward increase from 7‰ to 10‰ between 11°S and 15°S during the CWP (Fig. 4b). Thus, we suggest that the net increase in $\delta^{15}N_{bulk}$ from North to South during the CWP resembles the increase observed in modern surface sediments (Figs. 2 and 5a). However, unlike todays surface sediment data, the cores at 11°S and 12°S show substantially higher $\delta^{30}Si_{BSi}$ values during the CWP. According to the steady state calculations (3) this reflects high $Si(OH)_4$ utilization of up to 100%, whereas the NO_3^- utilization only reaches 80% at maximum (Fig. 5a).

Based on the classification of Fleury et al. 2015, we further distinguished between samples from humid periods (El Niño-like conditions) and arid periods (La Niña-like conditions) for the LIA (Figs. 4 and 5). This differentiation clearly highlights that samples from LIA (arid) phases are similar to samples from the CWP with $\delta^{15}NO_3^-$ source signatures of 8‰ to 9‰ between 11°S and 15° S, respectively. The shift towards a higher 1:2 NO_3^-:$Si(OH)_4$ utilization during both the CWP and LIA (arid) indicates enhanced utilization of $Si(OH)_4$ over NO_3^- leading to $Si(OH)_4$ limitation as indicated by high $Si(OH)_4$ utilization rates between 40% and 90%, whereas NO_3^- utilization rates were a bit lower around 25% to 80% (Fig. 5b). Such a decoupling of Si and N within diatoms can be caused by biogeochemical changes, such as iron availability altering the Si:N uptake dynamics (Hutchins and Bruland, 1998; Takeda, 1998) whereby elevated Si:N ratios are characteristic for Fe-limited diatom communities (Takeda, 1998). Accordingly, increased uptake of Si over N can lead to a $Si(OH)_4$ limitation as found during the CWP and LIA arid phases at 11°S to 12°S. The reason may have been that less Fe was upwelled at the narrow shelf between 11°S and 16°S, which led to Fe-limitation during progressing diatom blooms (Doering et al., 2016).

During the humid phases of the LIA the data indicate a lower $\delta^{15}NO_3^-$ source values around 6‰ for samples between 11°S and 12 °S and 7.5‰ further south between 14°S and 15°S (Fig. 4d). Additionally, the $\delta^{30}Si_{BSi}$ and $\delta^{15}N_{bulk}$ data plot below the 1:1 utilization line and between the utilization lines representing ratios of 2:1 and 15:1 for NO_3^-:$Si(OH)_4$. The calculated $Si(OH)_4$ utilization is

lowered to 6-60% and NO_3^- utilization increased to 70-90% (Fig. 5c). Also, while $\delta^{30}Si_{BSi}$ values remain remarkably stable (around 0.5‰ at 14°S; 0.7-1‰ at 11°S, 12°S and 15°S; with the exception of one higher data point at 11°S), $\delta^{15}N_{bulk}$ values show a wide range between 4.8‰ and 6.7‰ potentially reflecting enhanced NO_3^- limitation prevailing during these humid phases. The shift towards increasing $\delta^{15}N_{bulk}$ values with consistently low $\delta^{30}Si_{BSi}$ values can be caused by weaker denitrification due to the higher subsurface oxygenation (only suboxic and not anoxic conditions) reconstructed for the area together with decreased upwelling conditions at the time (Salvatteci et al., 2014b; Sifeddine et al., 2008). Unfortunately, to date there are no isotopic measurements available for either present day El-Niño $\delta^{15}NO_3^-$ or $\delta^{30}Si(OH)_4$ signatures of Peruvian water masses in order to better evaluate the effects of these significant changes in climatic forcing. Overall, our results indicate much higher NO_3^- utilization over $Si(OH)_4$ utilization (Fig. 5c), which is in agreement with phytoplankton assemblage analyses during El-Niño events indicating dominating productivity of non-siliceous phytoplankton groups (Sanchez et al., 2000). Accordingly, primary productivity dominated by non-siliceous phytoplankton leads to enhanced NO_3^- over $Si(OH)_4$ uptake. Although similar conditions are found offshore the Peruvian shelf today, these surface waters originate from the shelf area where diatom blooms prevail, thus being already depleted in $Si(OH)_4$ and not providing an adequate analogue for the conditions observed during the LIA.

However, while NO_3^- limitation seems to have prevailed at all latitudes during the LIA (humid) (i.e. all sample fall between the 2:1 and 15:1 utilization lines), only the data at 11-12°S indicates a $\delta^{15}NO_3^-$ source value close to 6‰. In contrast samples from 14-15°S show slightly higher $\delta^{15}N_{bulk}$ values up to 7.3 ± 0.1‰, potentially indicating a slight increase in $\delta^{15}NO_3^-$ to up to 7.5‰ due to ongoing but decreased denitrification at 14 to 15°S during this time. It should be noted that it was not possible to calculate $\delta^{15}NO_3^-$ values based on the linear function (eq. (2)) during this period, due to near horizontal alignment. Alternatively, we cannot exclude that under El-Niño-like conditions, the hydrodynamic conditions off Peru may be better described by a Rayleigh-type model (closed system) instead of the steady state model, which was reported to better describe the modern conditions (Ehlert et al., 2012). Applying a Rayleigh-type model calculation, $\delta^{15}N_{bulk}$ values of 7.3‰ during the LIA (humid) would reflect approximately 75% utilization assuming the $\delta^{15}NO_3^-$ source value remaining at 6‰ and an enrichment factor of -5‰. As upwelling of nutrient-rich water masses was diminished during this time, a closed system scenario is possibly to be more appropriate to interpret the isotopic signatures and would be in agreement with a more oxygenated (suboxic) water-column at the time reducing subsurface denitrification (Briceño-Zuluaga et al., 2016; Gutiérrez et al., 2009; Salvatteci et al., 2014b; Sifeddine et al., 2008). However, due to the lack of modern data for comparison with El-Niño events for comparison we assume a decrease to a $\delta^{15}NO_3^-$ source value of 6‰ between 11°S and 12°S and 7.5‰ between 14°S and 15°S during the LIA (humid) for the following discussion, still indicating a slight southward increase given that denitrification was not shut down completely (suboxic conditions as indicated by trace metal studies; Salvatteci et al., 2014b; Sifeddine et al., 2008) .

Biogeosciences Discuss., https://doi.org/10.5194/bg-2018-118
Manuscript under review for journal Biogeosciences
Discussion started: 9 April 2018

340 **3.2.2 Latitudinal variation in nutrient supply during the CWP and LIA**

341 Comparison of $\delta^{30}Si_{BSi}$ and $\delta^{15}N_{bulk}$ for the past ~600 years indicates that the source values for $\delta^{15}NO_3^-$
342 between 11°S and 15°S during the CWP and LIA (arid) were comparable to today yielding southward
343 increasing values of 7‰ to 10‰ caused by subsurface denitrification under oxygen-depleted
344 conditions (Fig. 2; Fig. 5a,b). In contrast, during the LIA (humid) the decrease in productivity and
345 upwelling have led to more oxygenated waters and subsequent reduction in denitrification devoid of a
346 strong increase in subsurface $\delta^{15}NO_3^-$, which was presumably closer to 6‰ and similar to that of the
347 PCUC reaching the northern shelf area today. Only at 14°S and 15°S the subsurface $\delta^{15}NO_3^-$ signal
348 may have been slightly increased by 1.5‰ due to denitrification if assuming that NO_3^- fractionation in
349 the hydrographic system of the area was continuously consistent with a steady-state type model over
350 time (Fig. 5c).

351 Based on these calculated subsurface $\delta^{15}NO_3^-$ values we further calculated the change in
352 nutrient utilization as well as nutrient supply for the different latitudes. Past nutrient utilization was
353 calculated following equation (2). Given the estimate of nutrient demand and export productivity it is
354 further possible to estimate changes in the supply with the relationship Δsupply =
355 Δdemand/Δutilization by applying the equation of Horn et al. (2011) given by:

356 (4) $$Nutrient\ supply = \frac{F_{BSi/TN}^{sample} / F_{BSi/TN}^{present}}{\%nutrient_{consumed}^{sample} / \%nutrient_{consumed}^{present}}$$

357 $F_{opal/TN}$ is the flux of BSi or TN and $\%nutrient_{consumed}$ is the percent of the $Si(OH)_4$ or NO_3^- supply
358 consumed (i.e. nutrient utilization). Given that there are no accumulation rates available for either the
359 surface sediment samples or for any of the cores to determine the export productivity directly, we used
360 the BSi and TN (wt%) values for calculation and not flux values. This may lead to an overestimation of
361 nutrient supply, but should reflect the correct trends. For the different time periods mean values for BSi
362 and TN were calculated and the respective nutrient supply was calculated based on equation (4),
363 indicating changes in the nutrient supply compared to modern values.

364 Generally, TN values are slightly lower during the CWP than today and lowest during the
365 LIA, with little difference between humid and arid phases. BSi concentrations are generally higher by
366 about 5% during the CWP and LIA (arid) with highest values at 15°S, and more similar values to today
367 during the LIA (humid) (Figs. 2, 5). When comparing modern (Fig. 2a) with mean $\delta^{30}Si_{BSi}$ and $\delta^{15}N_{bulk}$
368 values for the CWP (Fig. 5a) we observe a similar southward increase of both $\delta^{30}Si_{BSi}$ and $\delta^{15}N_{bulk}$
369 values, with generally slightly higher (0.1-0.2‰) $\delta^{30}Si_{BSi}$ values and with slightly lighter (0.5-1‰)
370 mean $\delta^{15}N_{bulk}$ values than today. A similar trend is observed during the LIA (arid) where $\delta^{15}N_{bulk}$ also
371 reach values of up to 7.9‰ at 15°S, while $\delta^{30}Si$ values are more variable and are even higher (0.4-
372 0.5‰) at 11°S and 12°S than modern values. For both the CWP and LIA (arid) calculated nutrient
373 utilization indicates higher $Si(OH)_4$ utilization (ranging between 30 and 100%) over NO_3^- utilization
374 (ranging between 20 and 90%), similar to modern utilization at 10-15°S (Figs. 2, 5). However, $Si(OH)_4$
375 utilization was even higher and NO_3^- utilization lower than modern values. The calculated Si and N
376 supplies both indicate a slight increase compared to today with Si supply increasing and N supply

377 decreasing towards 14°S and 15°S. The latter is in agreement with continuous denitrification in the
378 South causing loss of NO_3^-.

379 During the LIA (humid) $\delta^{30}Si_{BSi}$ values were consistently lower (0.3-0.5‰) than modern
380 values at all latitudes with the only higher values (0.2‰) found at 11°S. The $\delta^{15}N_{bulk}$ values remain
381 close to 5‰, only increasing up to 6.7‰ at 15°S, representing lighter values (0.6- 3‰) than today, in
382 agreement with the assumption of weakened N-loss processes during this time. The calculated nutrient
383 utilization shows a shift to high NO_3^- utilization (70-90%) and strongly diminished $Si(OH)_4$ utilization
384 (6-60%; Fig. 5c). These values are comparable to modern ones from the northern shelf (EQ-10°S),
385 where less nutrients are upwelled and productivity is lower (Ehlert et al., 2012). The calculated NO_3^-
386 supply was lowest during the LIA (humid) with little change over latitude in accordance with
387 prevalence of more oxygenated waters, whereas the Si supply strongly increased especially at 12°S
388 (Fig. 5c). However, the calculated increased $Si(OH)_4$ supply reflects the change in nutrient uptake (i.e.
389 nutrient ratio) due to stratification and potentially Fe limitation rather than an actual increase in
390 $Si(OH)_4$ supply reaching surface waters. Accordingly we observe a high $Si(OH)_4$ supply but low
391 utilization, thus indicating a low $Si(OH)_4$ demand at the time. In contrast NO_3^- supply appears to be
392 lower than today but the strongly enhanced NO_3^- utilization indicates a higher NO_3^- demand. This shift
393 towards a decreased $Si(OH)_4$ but an increased NO_3^- demand further supports a change in the nutrient
394 uptake ratio by phytoplankton (NO_3^-: $Si(OH)_4$ = 2:1 or 15:1, Fig. 4d). This is in agreement with
395 observations from modern El-Niño events, which show a shift in surface productivity from siliceous
396 (diatoms) to non-siliceous (dinoflagellates) phytoplankton (Sanchez et al., 2000).
397
398 Overall we find that the CWP, characterized by high upwelling intensity, productivity and N-loss
399 processes (Fleury et al., 2015; Salvatteci et al., 2014b; Sifeddine et al., 2008), is associated with
400 southward increasing $\delta^{30}Si_{BSi}$ and $\delta^{15}N_{bulk}$ values, reflecting moderate NO_3^- utilization and moderate to
401 high $Si(OH)_4$ utilization (Fig. 6, left). Highest $\delta^{30}Si_{BSi}$ and utilization values at 15°S are potentially
402 caused by progressive Fe limitation during diatom blooms, causing a NO_3^-:$Si(OH)_4$ ratio of up to 1:2.
403 Southward increasing $\delta^{15}N_{bulk}$ values and calculated $\delta^{15}NO_3^-$ demonstrate the consistent incorporation
404 of higher isotopic compositions due to subsurface denitrification under anoxic subsurface conditions in
405 agreement with decreasing NO_3^- supply illustrating the N-loss process. Similar conditions prevailed
406 during the sporadic periods of arid conditions observed during the LIA.

407 In contrast, most of the LIA i.e., the humid phases, was characterized by low productivity and
408 weak denitrification intensity between 10°S and 15°S (Díaz-Ochoa et al., 2009; Salvatteci et al., 2014b;
409 Sifeddine et al., 2008), with no significant southward increase in the source value of $\delta^{15}NO_3^-$ (Fig. 6,
410 right). Accordingly, high $\delta^{15}N_{bulk}$ and little change in NO_3^- supply indicate more complete NO_3^-
411 utilization during the LIA, while $\delta^{30}Si_{BSi}$ signatures and utilization remained low and Si supply high.
412 This indicates a shift towards a dominance of non-siliceous phytoplankton productivity causing NO_3^-
413 limitation and low uptake of Si similar to observations during modern El-Niño events, which are
414 characterized by a deepening of the thermocline and thus decreased nutrient delivery to surface waters.

Biogeosciences Discuss., https://doi.org/10.5194/bg-2018-118
Manuscript under review for journal Biogeosciences
Discussion started: 9 April 2018

Conclusions

Based on a compilation of new and previously published $\delta^{30}Si_{BSi}$ and $\delta^{15}N_{bulk}$ records of several short sediment cores from the southern Peruvian shelf (11-15°S) we present a new evaluation of the impact of denitrification on the isotopic source signature for NO_3^- and subsequent utilization. As denitrification increases southward along the shelf today, we applied a latitudinal correlation between $\delta^{30}Si_{BSi}$ and $\delta^{15}N_{bulk}$ signatures in modern surface and latest Holocene sediments. Given that the correlation of both proxies during the last 600 years is mainly influenced by nutrient utilization we performed a novel calculation of subsurface $\delta^{15}NO_3^-$ based on the linear correlation of $\delta^{30}Si_{BSi}$ and $\delta^{15}N_{bulk}$ signatures from the CWP and LIA (arid and humid conditions). Our results show that during the CWP and sporadic arid conditions during the LIA the isotopic compositions of NO_3^- have increased southward from 7‰ to 10‰ due to subsurface denitrification, similar to modern conditions. Furthermore, nutrient utilization was characterized by enhanced $Si(OH)_4$ over NO_3^- uptake, reflecting strong diatom blooms as observed today, potentially leading to progressive Fe limitation increasing the Si:N uptake ratio of diatoms to 2:1.

Low productivity and higher subsurface oxygenation (suboxic conditions) during the humid phases of LIA were associated with low $\delta^{30}Si_{BSi}$ and $\delta^{15}N_{bulk}$ signatures. The latitudinal comparison of $\delta^{30}Si_{BSi}$ versus $\delta^{15}N_{bulk}$ signatures supports decreased influence of subsurface denitrification on the NO_3^- isotope distribution with lower and more uniform $\delta^{15}NO_3^-$ source signatures between 6 and 7.5‰. However, NO_3^- utilization was significantly higher, while $Si(OH)_4$ utilization was lower and the Si supply was higher compared with the demand. This change in nutrient utilization is reflected by a NO_3^- :$Si(OH)_4$ uptake ratio of 2:1 to 15:1, suggesting a shift from a diatom-dominated regime to one dominated by non-siliceous phytoplankton. This is in agreement with El-Niño-like conditions prevailing during most of the LIA accompanied by a deepening of the thermocline and lower nutrient availability.

Overall, we are able to further improve the application of combined $\delta^{30}Si_{BSi}$ and $\delta^{15}N_{bulk}$ signatures as a powerful tool to differentiate between past changes in subsurface denitrification, nutrient utilization and supply but also changes in the nutrient ratio caused by either micro-(Fe) or macro-nutrient limitation.

Acknowledgement

This work is a contribution of the Collaborative Research Project 754 “Climate-Biogeochemistry interactions in the Tropical Ocean” (www.sfb754.de), which is supported by the Deutsche Forschungsgemeinschaft (DFG).

Biogeosciences Discuss., https://doi.org/10.5194/bg-2018-118
Manuscript under review for journal Biogeosciences
Discussion started: 9 April 2018

452 **Table 1: Downcore record of core M77/2-024-5TC, M77/2-005-3TC and M77/2-003-2TC for $\delta^{30}Si_{BSi}$ (‰)**
453 **and BSi content (wt%). The 2 SD represents the external reproducibilities of repeated sample**
454 **measurements.**

Core	Age yrs BP	Depth (mm)	BSi (wt %)	$\delta^{30}Si_{BSi}$ (‰)	2SD
24-5TC	42	0	16.2	1.50	0.23
	101	42	16.1	1.26	0.17
	154	104	34.3	1.50	0.18
	170	134	29.3	1.43	0.15
	187	161	23.7	1.47	0.05
	243	213	30.7	1.35	0.21
	304	264	28.1	1.40	0.09
	376	301	21.0	1.38	0.16
	422	390	10.1	0.81	0.19
	441	432	24.6	1.51	0.16
	483	473	23.8	1.61	0.08
005-3TC	46	0	15.9	1.07	0.09
	73	35	15.0	1.37	0.11
	95	69	25.4	1.46	0.21
	217	128	18.8	1.03	0.18
	250	165	17.3	0.80	0.22
	259	185	15.1	0.93	0.13
	303	241	13.1	0.44	0.27
	340	296	14.0	0.50	0.15
	358	323	11.6	0.47	0.20
	450	369	14.5	1.24	0.24
	464	389	25.0	1.60	0.19
003-2TC	22	0	39.2	1.63	0.24
	146	97	40.5	1.48	0.05
	245	174	41.9	1.30	0.26
	288	208	20.8	0.65	0.23
	327	239	23.9	0.74	0.13
	411	304	19.4	0.73	0.27
	474	353	46.7	1.38	0.17
	581	437	29.1	0.63	0.12

455

456

457

Biogeosciences Discuss., https://doi.org/10.5194/bg-2018-118
Manuscript under review for journal Biogeosciences
Discussion started: 9 April 2018

458 **Figures**

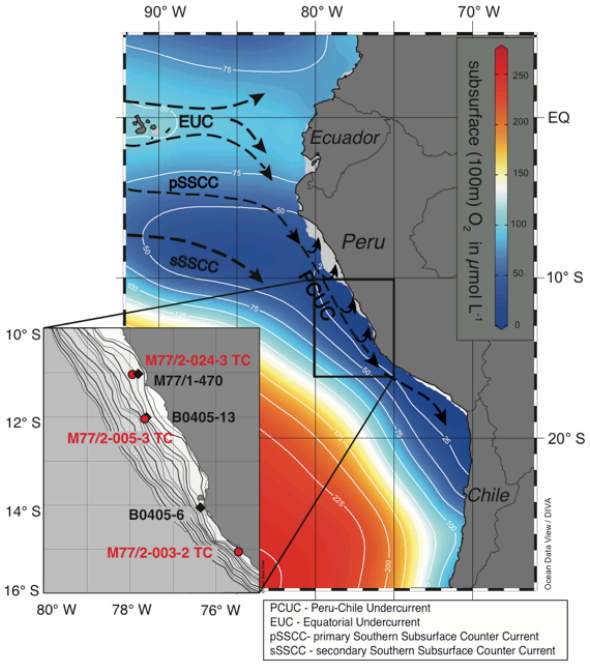

459

460 **Figure 1: (a) Subsurface (100 m) oxygen concentration and current directions in the Eastern Equatorial**
461 **Pacific. (b) Inset map shows locations of cores M77/2-024-3 TC, M77/2-005-3 TC, M77/2-003-2 TC (this**
462 **study) and M77/1-470, B0405-13 and B0405-6 (Ehlert et al., 2015; Gutiérrez et al., 2009) in more detail. The**
463 **bathymetry is given for 0 to 1000 m water depth in 50 m increments.**

464

465

466

467

468

Biogeosciences Discuss., https://doi.org/10.5194/bg-2018-118
Manuscript under review for journal Biogeosciences
Discussion started: 9 April 2018

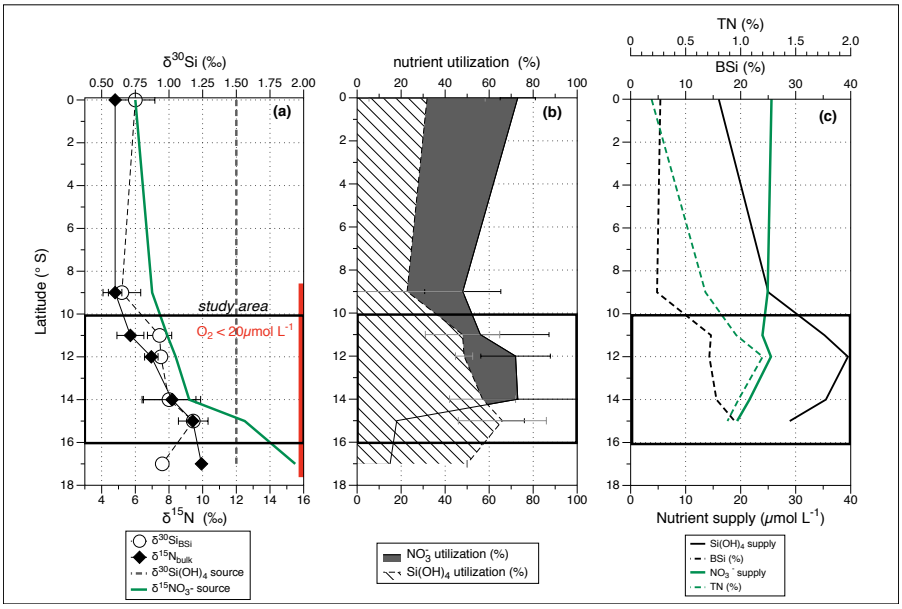

Figure 2: Latitudinal overview of present day (a) mean $\delta^{15}N_{bulk}$ (‰, black diamonds, 2 SD error bars) and $\delta^{30}Si_{BSi}$ (‰, white circles, 2SD error bars), the black dashed line indicates the subsurface $\delta^{30}Si(OH)_4$ source value of 1.5 ‰, the green solid line the $\delta^{15}NO_3^-$ source value, increasing southwards from 6‰ (EQ-8°S), to about 8‰ (10-12°S) and 12.5‰ (15°S). The red bar indicates the area of suboxic conditions in subsurface waters. The black rectangle marks the study area for downcore reconstruction (see also Fig.1). (b) Nutrient utilization for NO_3^- (%, dark grey area) and $Si(OH)_4$ (%, dashed area). (c) BSi (%, black dashed line), TN (%, green dashed line) and subsurface nutrient concentrations (= supply; in µmol L^{-1}, $Si(OH)_4$: black line; NO_3^-: green line). (Modified from Doering et al., 2016; Ehlert et al., 2012; Mollier-Vogel et al., 2012).

Biogeosciences Discuss., https://doi.org/10.5194/bg-2018-118
Manuscript under review for journal Biogeosciences
Discussion started: 9 April 2018

Biogeosciences
Discussions
Open Access
EGU

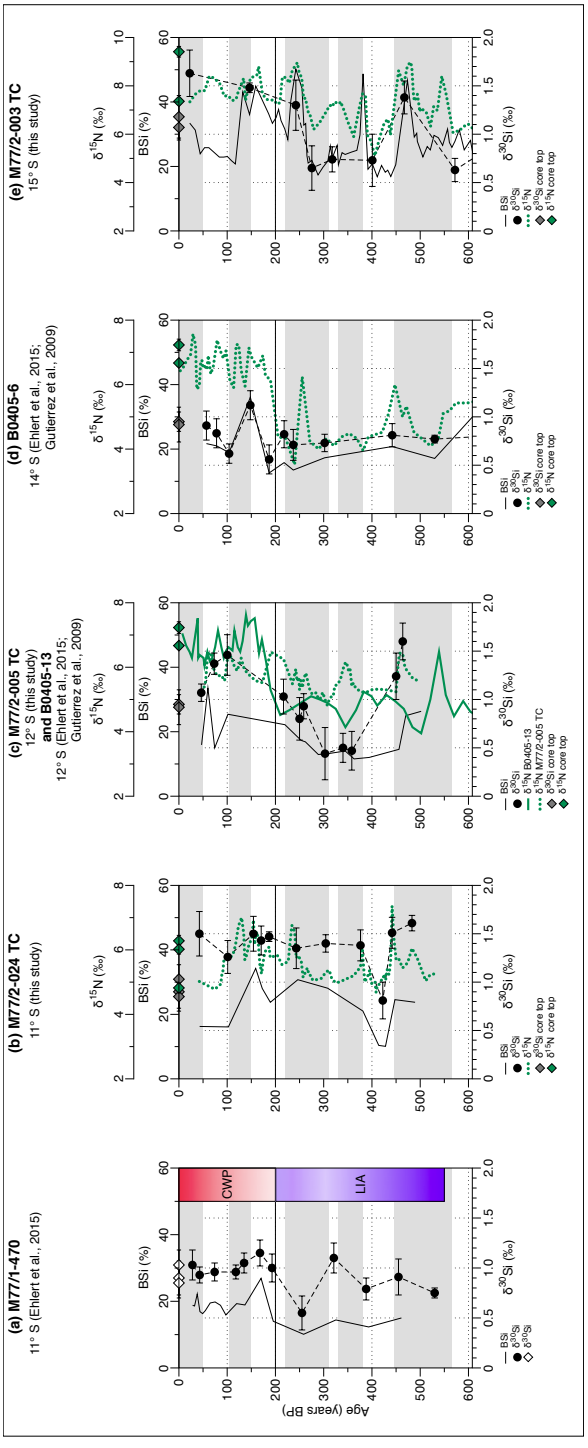

Figure 3: Downcore records of BSi (wt%), $\delta^{30}Si_{BSi}$ (‰, 2 SD error bar of repeated sample measurements) and $\delta^{15}N_{bulk}$ (‰) records of cores: (a) M77/1-470 (Ehlert et al., 2015), (b) M77/2-024-5TC, (c) M77/2-005-3TC and BO405-13 ($\delta^{15}N_{bulk}$ Gutiérrez et al., 2009), (d) BO405-6 ($\delta^{30}Si_{BSi}$ Ehlert et al., 2015; $\delta^{15}N_{bulk}$ Gutiérrez et al., 2009) and (e) M77/2-003-2TC. Records are sorted by latitude from left (11°S) to right (15°S). The time intervals for the CWP (red) and the LIA (blue) are highlighted in (a); the horizontal grey shading indicates humid periods (Fleury et al., 2015).

Biogeosciences Discuss., https://doi.org/10.5194/bg-2018-118
Manuscript under review for journal Biogeosciences
Discussion started: 9 April 2018

Biogeosciences
Discussions
Open Access
EGU

542

543 **Figure 4: (a) Correlation of $\delta^{15}N_{bulk}$ versus $\delta^{30}Si_{BSi}$ for**
544 **modern surface sediments (modified from Ehlert et al.,**
545 **2015), the dashed lines indicate 1:1 utilization of**
546 **different $\delta^{15}NO_3^-$ source values (7‰, 7.9‰, 8.35‰ and**
547 **11.3‰) between 9°S and 15°S (based on Mollier-Vogel**
548 **et al., 2012), the rectangle marks the respective range of**
549 **isotope values that can be expected in sediment samples**
550 **for nutrient utilization with source values of 1.5‰**
551 **($\delta^{30}Si(OH)_4$) and 8.35‰; (inset) Schematic overview of**
552 **nutrient utilization associated with changes in the**
553 **isotopic compositions of both $\delta^{15}N$ and $\delta^{30}Si$: the black**
554 **star marks the source signature (or 100% utilization)**
555 **for $\delta^{15}N$ and for $\delta^{30}Si$, the grey star marks the**
556 **respective isotopic compositions for 0% utilization, the**
557 **black dashed line indicates the 1:1 utilization for NO_3^-**
558 **:$Si(OH)_4$, respectively. Ratios that plot above the**
559 **utilization lines reflect $Si(OH)_4$ limitation, as indicated**
560 **by the dark grey and light grey dotted line representing**
561 **ratios of 1:2 and 1:4, whereas data points below record**
562 **stronger NO_3^- limitation, as indicated by the dark grey**
563 **and light grey dashed lines representing ratios of 2:1**
564 **and 15:1. The rectangle indicates the whole range of**
565 **possible isotopic values. (c-e) Downcore correlation of**
566 **$\delta^{15}N_{bulk}$ and $\delta^{30}Si_{BSi}$ for cores 024TC (diamonds),**
567 **005TC (grey stars), 003TC (grey squares) and BO405-6**
568 **(grey triangles; Ehlert et al., 2015), for the CWP and**
569 **the LIA. For the LIA the sample values are separated**
570 **into arid (d) and humid periods (e).**
571

572

573

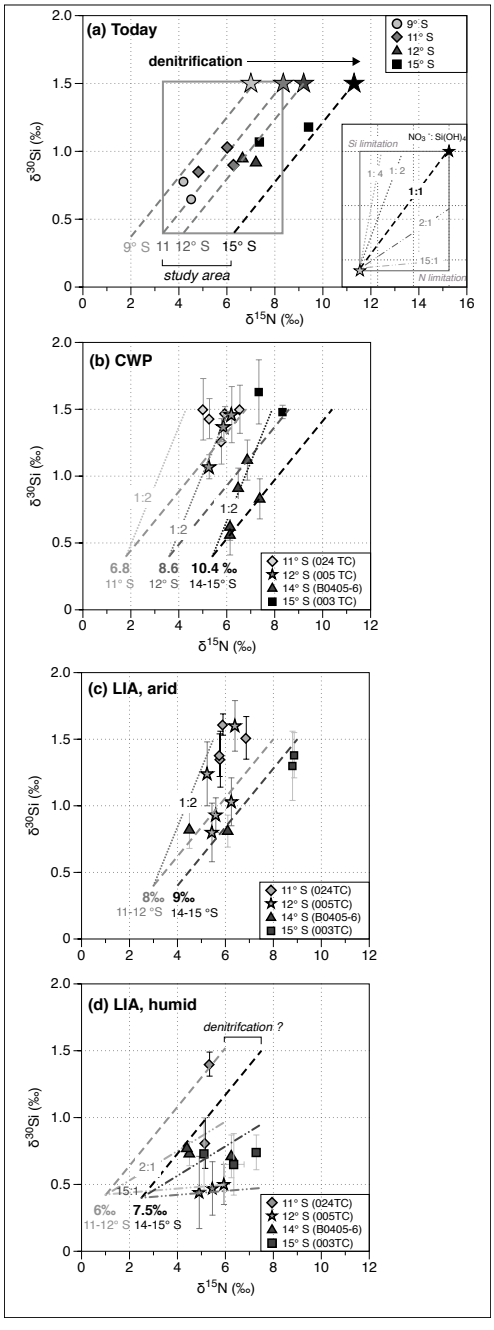

Biogeosciences Discuss., https://doi.org/10.5194/bg-2018-118
Manuscript under review for journal Biogeosciences
Discussion started: 9 April 2018

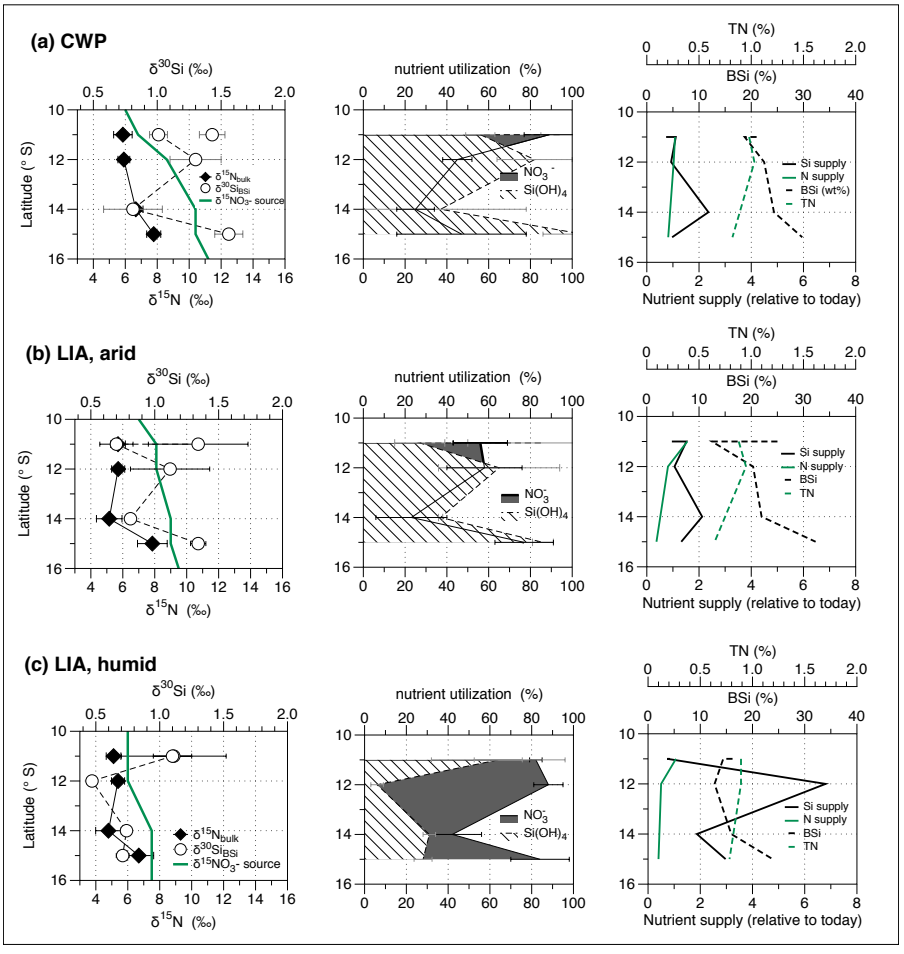

574

575 **Figure 5: Latitudinal comparison of (left) mean $\delta^{15}N_{bulk}$ (‰, black diamonds) and $\delta^{30}Si_{BSi}$ (‰, white circles)**
576 **and the calculated $\delta^{15}NO_3^-$ source values (green line), (middle) the respective nutrient utilization of NO_3^-**
577 **(grey, solid line) and $Si(OH)_4$ (dashed area and line) and (right) TN (%) and BSi (%) and nutrient supply**
578 **relative to today for (a) the CWP, (b) the arid phases of the LIA and (c) the humid phases of the LIA.**
579 **Please note that for $\delta^{15}N_{bulk}$ values the mean was calculated for all available values for each time period and**
580 **not only for samples, for which also $\delta^{30}Si_{BSi}$ values are available. Error bars mark the 1 SD of the mean**
581 **values.**

Biogeosciences Discuss., https://doi.org/10.5194/bg-2018-118
Manuscript under review for journal Biogeosciences
Discussion started: 9 April 2018

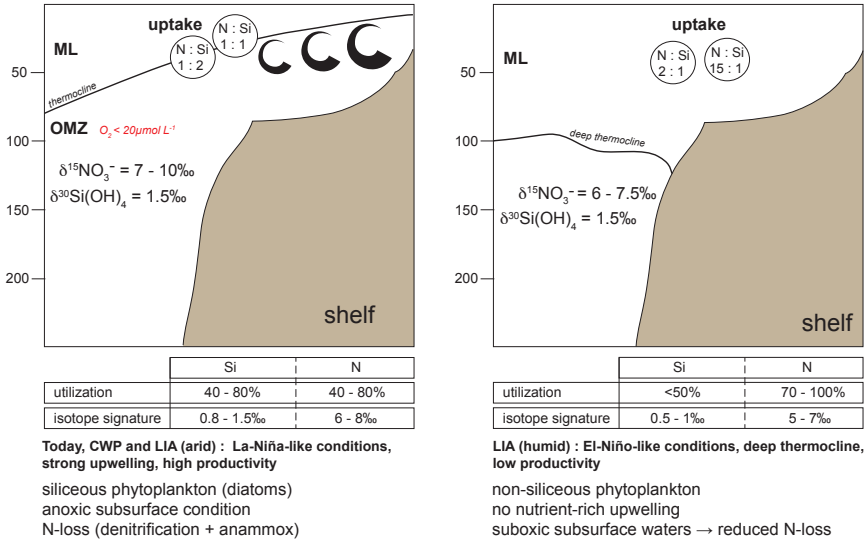

Figure 6: Schematic nutrient ($Si(OH)_4$ and NO_3^-) cycle models for the Peruvian shelf area (0-200m water depth) during the last 600 years. The NO_3^-:$Si(OH)_4$ (N:Si) indicates the ratio in which both nutrients are taken up during productivity in surface waters.

606 **References**

607 Agnihotri, R., Altabet, M. A. and Herbert, T. D.: Influence of marine denitrification on atmospheric
608 N_2O variability during the Holocene, Geophys. Res. Lett., 33(13), L13704,
609 doi:10.1029/2006GL025864, 2006.

610 Agnihotri, R., Altabet, M. A., Herbert, T. D. and Tierney, J. E.: Subdecadally resolved
611 paleoceanography of the Peru margin during the last two millennia, Geochem. Geophys. Geosyst., 9(5),
612 Q05013, doi:10.1029/2007GC001744, 2008.

613 Albarède, F., Telouk, P., Blichert-Toft, J., Boyet, M., Agranier, A. and Nelson, B.: Precise and accurate
614 isotopic measurements using multiple-collector ICPMS, Geochimica et Cosmochimica Acta, 68(12),
615 2725–2744, doi:10.1016/j.gca.2003.11.024, 2004.

616 Altabet, M. A., Deuser, W. G., Honjo, S. and Stienen, C.: Seasonal and Depth-Related Changes in the
617 Source of Sinking Particles in the North-Atlantic, Nature, 354(6349), 136–139, 1991.

618 Beucher, C. P., Brzezinski, M. A. and Jones, J. L.: Mechanisms controlling silicon isotope distribution
619 in the Eastern Equatorial Pacific, Geochimica et Cosmochimica Acta, 75(15), 4286–4294,
620 doi:10.1016/j.gca.2011.05.024, 2011.

621 Briceño-Zuluaga, F. J., Sifeddine, A., Caquineau, S., Cardich, J., Salvatteci, R., Gutiérrez, D., Ortlieb,
622 L., Velazco, F., Boucher, H. and Machado, C.: Terrigenous material supply to the Peruvian central
623 continental shelf (Pisco, 14° S) during the last 1000 years: paleoclimatic implications, Clim. Past,
624 12(3), 787–798, doi:10.5194/cp-12-787-2016, 2016.

625 Brink, K. H., Halpern, D., Huyer, A. and Smith, R. L.: The Physical-Environment of the Peruvian
626 Upwelling System, Progress in Oceanography, 12(3), 285–305, 1983.

627 Brunelle, B. G., Sigman, D. M., Cook, M. S., Keigwin, L. D., Haug, G. H., Plessen, B., Schettler, G.
628 and Jaccard, S. L.: Evidence from diatom-bound nitrogen isotopes for subarctic Pacific stratification
629 during the last ice age and a link to North Pacific denitrification changes, Paleoceanography, 22(1),
630 PA1215, doi:10.1029/2005PA001205, 2007.

631 Brzezinski, M. A.: A switch from $Si(OH)_4$ to NO_3^- depletion in the glacial Southern Ocean, Geophys.
632 Res. Lett., 29(12), 1564, doi:10.1029/2001GL014349, 2002.

633 Chaigneau, A., Dominguez, N. and Eldin, G.: Near-coastal circulation in the Northern Humboldt
634 Current System from shipboard ADCP data, *Geophys. Res. Ocean*s, 118, 5251–5266,
635 doi:10.1002/jgrc.20328, 2013.

636 Clement, A. C., Seager, R. and Cane, M. A.: Suppression of El Niño during the Mid-Holocene by
637 changes in the Earth's orbit, Paleoceanography, 15(6), 731–737, 2000.

638 Cline, J. D. and Kaplan, I. R.: Isotopic fractionation of dissolved nitrate during denitrification in the
639 eastern tropical North Pacific Ocean, Marine Chemistry, 3(4), 271–299, 1975.

640 Codispoti, L. A.: An oceanic fixed nitrogen sink exceeding 400 Tg N a^{-1} vs the concept of homeostasis
641 in the fixed-nitrogen inventory, Biogeosciences Discuss., 3(4), 1203–1246, 2006.

642 De Pol-Holz, R., Ulloa, O., Lamy, F., Dezileau, L., Sabatier, P. and Hebbeln, D.: Late Quaternary
643 variability of sedimentary nitrogen isotopes in the eastern South Pacific Ocean, Paleoceanography,
644 22(2), PA2207, doi:10.1029/2006PA001308, 2007.

645 de Souza, G. F., Reynolds, B. C., Rickli, J., Frank, M., Saito, M. A., Gerringa, L. J. A. and Bourdon,
646 B.: Southern Ocean control of silicon stable isotope distribution in the deep Atlantic Ocean, Global
647 Biogeochem. Cycles, 26(2), 2035–2047, doi:10.1029/2011GB004141, 2012.

648 De La Rocha, C. L., Brzezinski, M. A. and DeNiro, M. J.: Fractionation of silicon isotopes by marine
649 diatoms during biogenic silica formation, Geochimica et Cosmochimica Acta, 61(23), 5051–5056,

1997.

De La Rocha, C. L., Brzezinski, M. A., DeNiro, M. J. and Shemesh, A.: Silicon-isotope composition of diatoms as an indicator of past oceanic change, Nature, 395(6703), 680–683, 1998.

De La Rocha, C. L., Hutchins, D. A., Brzezinski, M. A. and Zhang, Y.: Effects of iron and zinc deficiency on elemental composition and silica production by diatoms, Mar. Ecol. Prog. Ser., 195, 71–79, 2000.

DeMaster, D. J.: The Supply and Accumulation of Silica in the Marine-Environment, Geochimica et Cosmochimica Acta, 45(10), 1715–1732, 1981.

Díaz-Ochoa, J. A., Lange, C. B., Pantoja, S., De Lange, G. J., Gutiérrez, D., Muñoz, P. and Salamanca, M.: Fish scales in sediments from off Callao, central Peru, Deep Sea Research Part II: Topical Studies in Oceanography, 56(16), 1124–1135, doi:10.1016/j.dsr2.2008.09.015, 2009.

Doering, K., Ehlert, C., Grasse, P., Crosta, X., Fleury, S., Frank, M. and Schneider, R.: Differences between mono-generic and mixed diatom silicon isotope compositions trace present and past nutrient utilisation off Peru, Geochimica et Cosmochimica Acta, 177(C), 30–47, doi:10.1016/j.gca.2015.12.029, 2016.

Ehlert, C., Grasse, P. and Frank, M.: Changes in silicate utilisation and upwelling intensity off Peru since the Last Glacial Maximum - insights from silicon and neodymium isotopes, Quaternary Science Reviews, 72, 18–35, doi:10.1016/j.quascirev.2013.04.013, 2013.

Ehlert, C., Grasse, P., Gutiérrez, D., Salvatteci, R. and Frank, M.: Nutrient utilisation and weathering inputs in the Peruvian upwelling region since the Little Ice Age, Clim. Past, 11(2), 187–202, doi:10.5194/cp-11-187-2015-supplement, 2015.

Ehlert, C., Grasse, P., Mollier-Vogel, E., Böschen, T., Franz, J., de Souza, G. F., Ben C Reynolds, Stramma, L. and Frank, M.: Factors controlling the silicon isotope distribution in waters and surface sediments of the Peruvian coastal upwelling, Geochimica et Cosmochimica Acta, 99(C), 128–145, doi:10.1016/j.gca.2012.09.038, 2012.

Fleury, S., Martinez, P., Crosta, X., Charlier, K., Billy, I., Hanquiez, V., Blanz, T. and Schneider, R. R.: Pervasive multidecadal variations in productivity within the Peruvian Upwelling System over the last millennium, Quaternary Science Reviews, 125(C), 78–90, doi:10.1016/j.quascirev.2015.08.006, 2015.

François, R., Altabet, M. A. and Burckle, L. H.: Glacial to interglacial changes in surface nitrate utilization in the Indian sector of the Southern Ocean as recorded by sediment δ15N, Paleoceanography, 7(5), 589–606, 1992.

Graco, M. I., Purca, S., Dewitte, B., Castro, C. G., Morón, O., Ledesma, J., Flores, G. and Gutiérrez, D.: The OMZ and nutrient features as a signature of interannual and low-frequency variability in the Peruvian upwelling system, Biogeosciences, 14(20), 4601–4617, doi:10.5194/bg-14-4601-2017, 2017.

Grasse, P., Ehlert, C. and Frank, M.: The influence of water mass mixing on the dissolved Si isotope composition in the Eastern Equatorial Pacific, Earth and Planetary Science Letters, 380, 60–71, doi:10.1016/j.epsl.2013.07.033, 2013.

Grasse, P., Ryabenko, E., Ehlert, C., Altabet, M. A. and Frank, M.: Silicon and nitrogen cycling in the upwelling area off Peru: A dual isotope approach, Limnol. Oceangr., 1–16, doi:10.1002/lno.10324, 2016.

Gutiérrez, D., Sifeddine, A., Field, D. B., Ortlieb, L., Vargas, G., Chávez, F. P., Velazco, F., Ferreira, V., Tapia, P., Salvatteci, R., Boucher, H., Morales, M. C., Valdés, J., Reyss, J. L., Campusano, A., Boussafir, M., Mandeng Yogo, M., García, M. and Baumgartner, T.: Rapid reorganization in ocean biogeochemistry off Peru towards the end of the Little Ice Age, Biogeosciences, 6(5), 835–848, doi:10.5194/bg-6-835-2009, 2009.

696 Horn, M. G., Beucher, C. P., Robinson, R. S. and Brzezinski, M. A.: Southern ocean nitrogen and
697 silicon dynamics during the last deglaciation, Earth and Planetary Science Letters, 310(3-4), 334–339,
698 doi:10.1016/j.epsl.2011.08.016, 2011.

699 Hutchins, D. A. and Bruland, K. W.: Iron-limited diatom growth and Si: N uptake ratios in a coastal
700 upwelling regime, Nature, 393(6685), 561–564, 1998.

701 Lam, P., Lavik, G., Jensen, M. M., van de Vossenberg, J., Schmid, M., Woebken, D., Gutiérrez, D.,
702 Amann, R., Jetten, M. S. and Kuypers, M. M.: Revising the nitrogen cycle in the Peruvian oxygen
703 minimum zone, Proceedings of the National Academy of Sciences, 106(12), 4752–4757, 2009.

704 Mariotti, A., Germon, J. C., Hubert, P., Kaiser, P., Letolle, R., Tardieux, A. and Tardieux, P.:
705 Experimental determination of nitrogen kinetic isotope fractionation: some principles; illustration for
706 the denitrification and nitrification processes, Plant Soil, 62(3), 413–430, 1981.

707 Mollier-Vogel, E., Ryabenko, E., Martinez, P., Wallace, D., Altabet, M. A. and Schneider, R.: Nitrogen
708 isotope gradients off Peru and Ecuador related to upwelling, productivity, nutrient uptake and oxygen
709 deficiency, Deep-Sea Research Part I, 70(c), 14–25, doi:10.1016/j.dsr.2012.06.003, 2012.

710 Müller, P. J. and Schneider, R.: An Automated Leaching Method for the Determination of Opal in
711 Sediments and Particulate Matter, Deep-Sea Research Part I, 40(3), 425–444, 1993.

712 Pennington, J. T., Mahoney, K. L., Kuwahara, V. S., Kolber, D. D., Calienes, R. and Chavez, F. P.:
713 Primary production in the eastern tropical Pacific: A review, Progress in Oceanography, 69(2-4), 285–
714 317, doi:10.1016/j.pocean.2006.03.012, 2006.

715 Pichevin, L., Martinez, P., Bertrand, P., Schneider, R., Giraudeau, J. and Emeis, K.: Nitrogen cycling
716 on the Namibian shelf and slope over the last two climatic cycles: Local and global forcings,
717 Paleoceanography, 20(2), PA2006, doi:10.1029/2004PA001001, 2005.

718 Rafter, P. A., Sigman, D. M., Charles, C. D., Kaiser, J. and Haug, G. H.: Subsurface tropical Pacific
719 nitrogen isotopic composition of nitrate: Biogeochemical signals and their transport, Global
720 Biogeochem. Cycles, 26(1), GB1003, doi:10.1029/2010GB003979, 2012.

721 Reynolds, B. C., Frank, M. and Halliday, A. N.: Evidence for a major change in silicon cycling in the
722 subarctic North Pacific at 2.73 Ma, Paleoceanography, 23(4), PA4219, doi:10.1029/2007PA001563,
723 2008.

724 Robinson, R. S., Brzezinski, M. A., Beucher, C. P., Horn, M. G. S. and Bedsole, P.: The changing roles
725 of iron and vertical mixing in regulating nitrogen and silicon cycling in the Southern Ocean over the
726 last glacial cycle, Paleoceanography, 29(12), 1179–1195, doi:10.1002/2014PA002686, 2014.

727 Sachs, J. P., Sachse, D., Smittenberg, R. H., Zhang, Z., Battisti, D. S. and Golubic, S.: Southward
728 movement of the Pacific intertropical convergence zone AD 1400–1850, Nature Geoscience, 2(7), 519–
729 525, doi:10.1038/ngeo554, 2009.

730 Salvatteci, R., Field, D., Sifeddine, A., Ortlieb, L., Ferreira, V., Baumgartner, T., Caquineau, S.,
731 Velazco, F., Reyss, J.-L., Sanchez-Cabeza, J. A. and Gutiérrez, D.: Cross-stratigraphies from a
732 seismically active mud lens off Peru indicate horizontal extensions of laminae, missing sequences, and
733 a need for multiple cores for high resolution records, Marine Geology, 357(C), 72–89,
734 doi:10.1016/j.margeo.2014.07.008, 2014a.

735 Salvatteci, R., Gutiérrez, D., Field, D., Sifeddine, A., Ortlieb, L., Bouloubassi, I., Boussafir, M.,
736 Boucher, H. and Cetin, F.: The response of the Peruvian Upwelling Ecosystem to centennial-scale
737 global change during the last two millennia, Clim. Past, 10(2), 715–731, doi:10.5194/cp-10-715-2014-
738 supplement, 2014b.

739 Sanchez, G., Calienes, R. and Zuta, S.: The 1997-98 El Niño and its effects on the coastal marine
740 ecosystem off Peru, Reports of California Cooperative Oceanic Fisheries Investigations, 41, 62–86,
741 2000.

742 Sifeddine, A., Gutiérrez, D., Ortlieb, L., Boucher, H., Velazco, F., Field, D., Vargas, G., Boussafir, M.,
743 Salvatteci, R., Ferreira, V., García, M., Valdés, J., Caquineau, S., Mandeng Yogo, M., Cetin, F., Solis,
744 J., Soler, P. and Baumgartner, T.: Laminated sediments from the central Peruvian continental slope: A
745 500 year record of upwelling system productivity, terrestrial runoff and redox conditions, Progress in
746 Oceanography, 79(2-4), 190–197, doi:10.1016/j.pocean.2008.10.024, 2008.

747 Takeda, S.: Influence of iron availability on nutrient consumption ratio of diatoms in oceanic waters,
748 Nature, 393(6687), 774–777, 1998.

749 Toggweiler, J. R., Dixon, K. and Broecker, W. S.: The Peru Upwelling and the Ventilation of the
750 South-Pacific Thermocline, J. Geophys. Res., 96(C11), 20467–20497, 1991.

751 Wada, E. and Hattori, A.: Nitrogen isotope effects in the assimilation of inorganic nitrogenous
752 compounds by marine diatoms, Geomicrobiology Journal, 1(1), 85–101,
753 doi:10.1080/01490457809377725, 1978.

754 Waser, N., Harrison, P. J., Nielsen, B., Calvert, S. E. and Turpin, D. H.: Nitrogen isotope fractionation
755 during the uptake and assimilation of nitrate, nitrite, ammonium, and urea by a marine diatom, Limnol.
756 Oceangr., 43(2), 215–224, 1998.

757 Wilken, S., Hoffmann, B., Hersch, N., Kirchgessner, N., Dieluweit, S., Rubner, W., Hoffmann, L. J.,
758 Merkel, R. and Peeken, I.: Diatom frustules show increased mechanical strength and altered valve
759 morphology under iron limitation, Limnol. Oceangr., 56(4), 1399–1410,
760 doi:10.4319/lo.2011.56.4.1399, 2011.

761 Zuta, S. and Guillén, O.: Oceanografía de las aguas costeras del Perú, Bo. Inst. Mar. Perú, 2(5), 157–
762 324, 1970.

763